# Aeroelastic stability of a 3DOF system based on quasi-steady theory with reference to inertial coupling

He, Mingzhe; macdonal, john

*DOI:*
10.1016/j.jweia.2017.10.013

Journal of Wind Engineering & Industrial Aerodynamics 171 (2017) 319–329

Contents lists available at ScienceDirect

Journal of Wind Engineering & Industrial Aerodynamics

journal homepage: www.elsevier.com/locate/jweia

# Aeroelastic stability of a 3DOF system based on quasi-steady theory with reference to inertial coupling

Mingzhe He [*,1], John Macdonald

*Department of Civil Engineering, University of Bristol, BS8 1TR, UK*

ARTICLE INFO

*Keywords:*
3DOF galloping
Quasi-steady theory
Inertial coupling
Eigenvalue problem

ABSTRACT

This paper investigates the galloping stability of a two-dimensional three-degree-of-freedom (3DOF) system with an eccentric shape, such as an iced cable or power transmission line, incorporating inertial coupling along with the aerodynamic damping. The inertial coupling is a result of the offset of the centre of mass with respect to the elastic centre. A theoretical model is firstly constructed for the derivation of the aerodynamic damping matrix, based on quasi-steady theory, as well as the inertial coupling components in the mass matrix. The model is then employed to investigate the effects on the aeroelastic stability of the system of incorporating the inertial coupling and the results are compared with both dynamic test results and predictions from previous models. The comparisons indicate that even small eccentricity can lead to significant change of the stability of the system, for both detuned and perfectly tuned natural frequencies of the different degrees of freedom. For a system with perfectly tuned natural frequencies, and neglecting structural damping, analytical solutions of the eigenfrequencies and eigenvectors allowing for the inertial coupling, are derived for the case of no wind. Subsequently, an approximate solution is found for the prediction of the galloping stability of a system coupled by the aerodynamic damping as well as the inertial coupling. Finally, the approximate solution is verified against numerical results using examples with two cross-section shapes, showing excellent agreement.

## 1. Introduction

Galloping has been a major problem for decades for slender structures, especially transmission lines and bridge cables. One of the most common methods of predicting galloping is to use theoretical models, based on quasi-steady theory, which only requires static aerodynamic coefficients measured in wind tunnel tests. Den Hartog (1932) proposed a simple expression to forecast across-wind galloping of transmission lines with ice accretion, which is still widely used today. However, it is only valid for wind normal to the body and only considers the single-degree-of-freedom (1DOF) case.

It is common to consider aerodynamic couplings between the vertical and torsional motion of a section in flutter analysis. Flutter instability is a well-known phenomenon which could cause structural failure of aircraft wings, long-span bridges, etc. The stability is normally assessed by a numerical approach based on flutter derivatives which, similar to the aerodynamic coefficients, can also be measured in wind tunnel tests, but more dynamic tests must be involved. Chen and Kareem (2006) successfully derived a closed-form solution of coupled flutter instability of long-span bridges, which showed good agreement with test results. It should be noted that flutter derivatives are functions of reduced velocity, which is rather low for large bodies such as bridge decks, leading to a low accuracy of quasi-steady theory. However, if cross-sections with much smaller diameters are considered, such as cables and power lines, quasi-steady theory, as well as the term “galloping”, is more applicable. Also, the static aerodynamic coefficients are much easier to measure in comparison with flutter derivatives.

For iced transmission line conductors, Den Hartog proved that the ice accretion plays a significant role in modifying the aerodynamics, potentially leading to aerodynamic instability in the pure across-wind direction. However, if the torsional motion is also considered, the effects of inertial coupling due to the eccentric mass of the ice coating could be equally important. There has been extensive literature on two-degree-of-freedom (2DOF) galloping (coupled plunge and torsion), based on quasi-steady theory (Slater, 1969; Blevins and Iwan, 1974; Modi and Slater, 1983; Yu et al., 1995a, 1995b), as reviewed by Blevins (1994) and Païdoussis et al. (2010). Slater (1969) was the first to investigate this problem using a right angle section, with both aerodynamic and inertial

* Corresponding author.
*E-mail addresses:* m.he@bham.ac.uk (M. He), john.macdonald@bristol.ac.uk (J. Macdonald).
[1] Now at the University of Birmingham. Address: University of Birmingham, Civil Engineering Building; Engineering South Campus, Edgbaston, Birmingham, B15 2TT, UK.

https://doi.org/10.1016/j.jweia.2017.10.013
Received 27 April 2017; Received in revised form 10 October 2017; Accepted 11 October 2017

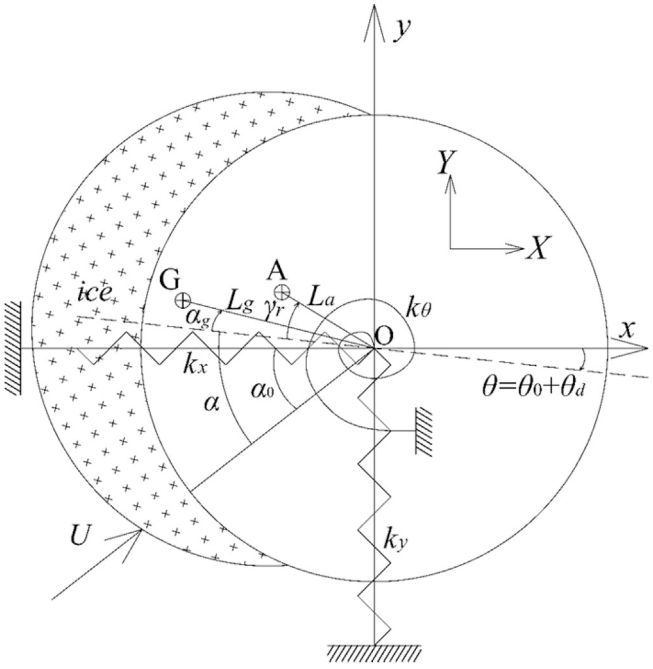


**Fig. 1.** The 2 dimensional model of the 3DOF system.

coupling. Interaction between torsion and plunge was expected, due to the misalignment of the mass centre and shear centre. However, only distinct vertical or torsional motion was identified in the dynamic experiments, which was believed to be because the inertial coupling was weak. A similar cross-section was also studied by Blevins and Iwan (1974), who neglected inertial coupling from the outset and focused on internally resonant and non-resonant cases. Yu et al. (1995a) used a 2DOF model representing a single conductor with ice coating to not only identify the onset of the coupled transverse-torsion galloping but also to investigate the significance of the eccentricity. In their companion work (Yu et al., 1995b), the methodology was applied to periodic motions. Although it is generally not possible to derive simple analytical solutions for such complicated problem, they managed to show the trends of the galloping onset threshold due to the eccentricity in a tabular manner for practical purposes.

Jones (1992) was the first to investigate the 2DOF translational galloping problem (along- and across-wind) experimentally and analytically for a perfectly tuned system and found that aerodynamic coupling between the two degrees of freedom was important. Macdonald and Larose (2006) generalised the Den Hartog criterion by allowing for Reynolds number effects and three-dimensional geometry of the inclined cable in a skew wind. They then extended it to apply to 2DOF translational galloping (Macdonald and Larose, 2008a,b). They provided a closed-form solution for the minimum structural damping required to prevent galloping of a system with the same natural frequencies in the two planes. The companion paper looked at some detuning cases based on numerical solutions. Meanwhile, Carassale et al. (2005) derived equivalent expressions of the aerodynamic damping matrix, but excluding and questioning the relevance of Reynolds number effects. Furthermore, Luongo and Piccardo (2005) proposed an analytical approximation for the onset of galloping of a 2DOF translational system with arbitrary natural frequencies, employing a perturbation approach. The above analyses were reviewed by Nikitas and Macdonald (2014). However, inertial coupling was not considered in any of them.

The afore-mentioned research implies that there could be interactions between heave, sway and torsion simultaneously, which poses the necessity of studying coupled 3DOF galloping. Yu et al. (1993a,b) developed the work by Jones (1992) and established a galloping threshold, based on the Routh-Hurwitz criterion, for a 3DOF system with mass eccentricity. Wang and Lilien (1998) studied single and bundled transmission lines covered by ice coating and similarly proposed a model taking all three degrees of freedom into account. However, both these studies concentrated on multi-span effects rather than a simple criterion for the onset of galloping. The Routh-Hurwitz criterion utilised by Yu et al. (1993a,b) is rather inefficient for determining how stable or unstable the system is. In the latter study, the galloping stability was evaluated by numerical time history analysis.

Very few dynamic wind tunnel tests on 2 or 3DOF galloping have been reported in the literature. Chabart and Lilien (1998) carried out both static and dynamic wind tunnel tests on a heavily iced cable which shed some light on the galloping mechanism of a 3DOF cable with large eccentricity. Gjelstrup and Georgakis (2011) extended the model by Macdonald and Larose (2008a, b) to include the torsional degree of freedom and also the case where the mass centre and elastic centre do not coincide. The theoretical galloping threshold was determined using the Routh-Hurwitz criterion and reasonable comparisons were found with the observations from the experiments by Chabart and Lilien (1998). Gjelstrup et al. (2012) further carried out some experiments to examine the galloping stability of bridge cables and hangers with various ice shapes. The test results were also compared with the theoretical model by Gjelstrup and Georgakis (2011). However, the experiments only allowed for vertical and torsional motions and mass eccentricity was not explicitly considered. More recent contributions on 3DOF galloping include work by Piccardo et al. (2014) who presented the full aerodynamic damping matrix in a more general form, while Demartino and Ricciardelli (2015) compared various existing quasi-steady models for galloping, using wind tunnel measurements for bridge cables and hangers with ice accretion, shedding some light on the application of each model. He and Macdonald (2016) extended the work by Nikitas and Macdonald (2014) and rigorously studied 3DOF galloping of a system coupled only by aerodynamic damping and proposed a simple closed-form solution for galloping of a perfectly tuned 3DOF system. They also numerically investigated the effects of the tuning of the structural natural frequencies (He and Macdonald, 2015).

The aim of this paper is to extend the previous 3DOF analytical model by He and Macdonald (2016) to include inertial coupling. Firstly, the inertial coupling terms in the mass matrix are derived in the same way as in Gjelstrup and Georgakis (2011). Then, the significance of the inertial coupling for the galloping behaviour is investigated. Subsequently, having found analytical solutions to the eigenvalue problem for an eccentric 3DOF system, without wind or structural damping, approximate analytical solutions are found for the galloping stability of the system in the presence of wind. Finally, the approximate analytical solutions are validated against conventional numerical solutions for the same system.

## 2. 3DOF model and equations of motion

Recently, He and Macdonald (2016) presented a 2-dimensional 3DOF model and derived the aerodynamic damping matrix in a simple form, including all three degrees of freedom, based on quasi-steady theory. Inertial coupling was excluded, implying coincidence of the elastic centre (O) and mass centre (G), which is applicable for sections with symmetrical geometry and lightly iced sections with a negligible offset of the centre of mass. A modified model is presented herein to include the inertia effects, as illustrated in Fig. 1, where G is offset from O. The incorporation of all three degrees of freedom results in a difficulty of quasi-steady theory, namely suitable treatment of the rotational velocity. The approach employed follows the common approach in the literature (Slater, 1969; Blevins and Iwan, 1974; Nakamura and Mizota, 1975; Blevins, 1994; Gjelstrup and Georgakis, 2011; He and Macdonald, 2016), where an aerodynamic centre is defined to emulate the effect of the rotational velocity on the aerodynamic forces using the wind velocity relative to that point.

Fig. 1 shows the definitions of all the geometric parameters. $x$ and $y$

indicate the directions of the principal structural axes of the system and $\theta$ is the rotation of the cross-section, measured between the $x$ axis and a reference line on the body (the dashed line in Fig. 1, fixed to the cross-sectional shape). $\theta$ consists of two parts, namely the static rotation of the shape, $\theta_0$ (e.g. due to the mean wind load or the weight of accreted ice), and the dynamic component, $\theta_d$. The structural stiffness of each degree of freedom is denoted $k_x$, $k_y$ and $k_\theta$, which can also be expressed as $m\omega_x^2$, $m\omega_y^2$ and $J_\theta\omega_\theta^2$, respectively. $m$ is the mass per unit length of the structure and $J_\theta$ is the polar mass moment of inertia per unit length about point O. $\omega_x$, $\omega_y$ and $\omega_\theta$ are the angular natural frequencies of the uncoupled structural system in each degree of freedom. $\alpha_0$ is the angle between the wind direction and the $x$ axis while $\alpha$ represents the angle between the wind direction and the body reference line ($\alpha = \alpha_0+\theta$). The mass centre (G) differs from the elastic centre (O), for example, due to the ice accretion, and is positioned at a radius $L_g$ at an angle $\alpha_g$ from the body reference line. Similarly, the offset distance and angle of the aerodynamic centre (A) from the elastic centre are respectively defined by $L_a$ and $\gamma_r$ from the reference line. It should be noted that the aerodynamic centre (A) in Fig. 1 is shown in an arbitrary position for illustration of the general case. The specific point used for the numerical examples later in the current paper is defined in Section 3.1.

The position of any point on the shape can be defined in the absolute coordinate system, indicated by $X$ and $Y$ axes in Fig. 1. The absolute coordinates of the centre of mass are:

$$X = x - L_g\cos(\alpha_g+\theta), \quad Y = y + L_g\sin(\alpha_g+\theta) \tag{1}$$

Hence,

$$\dot{X} = \dot{x} + L_g\dot{\theta}\sin(\alpha_g+\theta), \quad \dot{Y} = \dot{y} + L_g\dot{\theta}\cos(\alpha_g+\theta) \tag{2}$$

The equations of motion can then be obtained by applying the Euler-Lagrange equation, which involves the kinetic ($T$) and potential ($V$) energy, expressed as:

$$T = \frac{1}{2}m\left(\dot{X}^2+\dot{Y}^2\right) + \frac{1}{2}J_G\dot{\theta}^2 \tag{3}$$

$$V = \frac{1}{2}k_x x^2 + \frac{1}{2}k_y y^2 + \frac{1}{2}k_\theta\theta^2 \tag{4}$$

With the Lagrangian defined as $L = T\text{-}V$, the force on the body in the $x$ direction, excluding the damping component, satisfies:

$$F_x = \frac{\partial}{\partial t}\left(\frac{\partial L}{\partial \dot{x}}\right) - \frac{\partial L}{\partial x} \tag{5}$$

The force in the $y$ direction, $F_y$, and the moment on the body $F_\theta$, can be expressed similarly. Hence, the full equations of motion, with damping forces included, are:

$$F_x = m\ddot{x} + 2m\omega_x\zeta_x\dot{x} + k_x x + mL_g\left(\ddot{\theta}\sin(\alpha_g+\theta) + \dot{\theta}^2\cos(\alpha_g+\theta)\right) \tag{6}$$

$$F_y = m\ddot{y} + 2m\omega_y\zeta_y\dot{y} + k_y y + mL_g\left(\ddot{\theta}\cos(\alpha_g+\theta) - \dot{\theta}^2\sin(\alpha_g+\theta)\right) \tag{7}$$

$$F_\theta = J_\theta\ddot{\theta} + 2m\omega_\theta\zeta_\theta\dot{\theta} + k_\theta\theta + mL_g\ddot{x}\sin(\alpha_g+\theta) + mL_g\ddot{y}\cos(\alpha_g+\theta) \tag{8}$$

where $\zeta_x$, $\zeta_y$ and $\zeta_\theta$ are the structural damping ratios for each degree of freedom and $J_\theta = J_G + mL_g^2 = mr^2$ is the polar mass moment of inertia per unit length about point O, as mentioned earlier and $r$ is the radius of gyration about O. $J_G$ is the polar mass moment of inertia per unit length about point G. It should be noted that the terms associated with $\dot{\theta}^2$ can be neglected when linearising the force at the initial steady state condition.

The equations of motion can be written in matrix form as:

$$\mathbf{M}\ddot{\mathbf{x}} + \mathbf{C_s}\ddot{\mathbf{x}} + \mathbf{K}\mathbf{x} = \mathbf{F} \tag{9}$$

where

$$\mathbf{M} = m\begin{bmatrix} 1 & 0 & L_g\sin(\alpha_g+\theta) \\ 0 & 1 & L_g\cos(\alpha_g+\theta) \\ L_g\sin(\alpha_g+\theta) & L_g\cos(\alpha_g+\theta) & r^2 \end{bmatrix},$$

$$\mathbf{C_s} = \begin{bmatrix} 2m\omega_x\zeta_x & 0 & 0 \\ 0 & 2m\omega_y\zeta_y & 0 \\ 0 & 0 & 2J_\theta\omega_\theta\zeta_\theta \end{bmatrix}, \quad \mathbf{K} = \begin{bmatrix} m\omega_x^2 & 0 & 0 \\ 0 & m\omega_y^2 & 0 \\ 0 & 0 & J_\theta\omega_\theta^2 \end{bmatrix},$$

$$\mathbf{x} = \begin{Bmatrix} x \\ y \\ \theta_d \end{Bmatrix}, \mathbf{F} = \begin{Bmatrix} F_x \\ F_y \\ F_\theta \end{Bmatrix}.$$

Neglecting any applied forces other than the aerodynamic forces due to the motion of the body in the wind, and linearising the force vector with respect to the velocity vector, about the static equilibrium configuration (in where $\mathbf{x} = 0$), the force vector can be expressed as

$$\mathbf{F} = -\mathbf{C_a}\mathbf{x} \tag{10}$$

$\mathbf{C_a}$ is the aerodynamic damping matrix, given by:

$$\mathbf{C_a} = \begin{bmatrix} c_{xxa} & c_{xya} & c_{x\theta a} \\ c_{yxa} & c_{yya} & c_{y\theta a} \\ c_{\theta xa} & c_{\theta ya} & c_{\theta\theta a} \end{bmatrix} = \begin{bmatrix} -\frac{\partial F_x}{\partial \dot{x}} & -\frac{\partial F_x}{\partial \dot{y}} & -\frac{\partial F_x}{\partial \dot{\theta}} \\ -\frac{\partial F_y}{\partial \dot{x}} & -\frac{\partial F_y}{\partial \dot{y}} & -\frac{\partial F_y}{\partial \dot{\theta}} \\ -\frac{\partial F_\theta}{\partial \dot{x}} & -\frac{\partial F_\theta}{\partial \dot{y}} & -\frac{\partial F_\theta}{\partial \dot{\theta}} \end{bmatrix}_{\dot{x}=\dot{y}=\dot{\theta}=\theta_d=0} \tag{11}$$

which, based on quasi-steady theory and for any wind direction and orientation of the body, has been shown to be (He and Macdonald, 2016):

$$\mathbf{C_a} = \frac{\rho DU}{2}\begin{bmatrix} 2C_D & 2C_L & (C_L'+C_D) & (C_L-C_D') & 0 & 0 \\ 2C_L & -2C_D & (C_L-C_D') & -(C_L'+C_D) & 0 & 0 \\ 0 & 0 & 0 & 0 & 2DC_M & DC_M' \end{bmatrix} \times \begin{bmatrix} c^2 & cs & L_a s_{\alpha\theta\gamma}\, c \\ -cs & -s^2 & -L_a s_{\alpha\theta\gamma}\, s \\ s^2 & -cs & -L_a c_{\alpha\theta\gamma}\, s \\ cs & -c^2 & -L_a c_{\alpha\theta\gamma}\, c \\ c & s & L_a s_{\alpha\theta\gamma} \\ -s & c & L_a c_{\alpha\theta\gamma} \end{bmatrix} \tag{12}$$

where $\rho$ is the density of air, $D$ is a reference dimension of the body and $C_D$, $C_L$and $C_M$ are, respectively, the static drag, lift and moment coefficients of the cross-section, which are taken to be only functions of the angle of attack, $\alpha$. The primes indicate derivatives with respect to the angle of attack. In addition, $c = \cos\alpha_0$, $s = \sin\alpha_0$, $c_{\alpha\theta\gamma} = \cos(\alpha_0+\theta_0+\gamma_r)$ and $s_{\alpha\theta\gamma} = \sin(\alpha_0+\theta_0+\gamma_r)$.

The equations of motion and the asymmetric mass matrix due to eccentricity are equivalent to those derived by Gjelstrup and Georgakis (2011).

It should be emphasised that the force coefficients and their derivatives should be evaluated at the angle between the wind and the shape in the static equilibrium configuration about which the dynamic stability is considered, i.e. at $\alpha_0+\theta_0$ ($=\alpha$ for $\theta_d = 0$). To address the stability, i.e. the conditions for the onset of galloping, it is sufficient to use the linearised representation of the aerodynamic forces above.

He and Macdonald (2016) found that the determinant of the 3DOF quasi-steady aerodynamic damping matrix $\mathbf{C_a}$ is always zero, which is not generally true for any pair of two DOFs. The reason is that the motion of the aerodynamic centre due to the rotational velocity can be decomposed into components in the $x$ and $y$ directions, leading to the third column of the $3\times3$ aerodynamic damping matrix being a linear combination of the

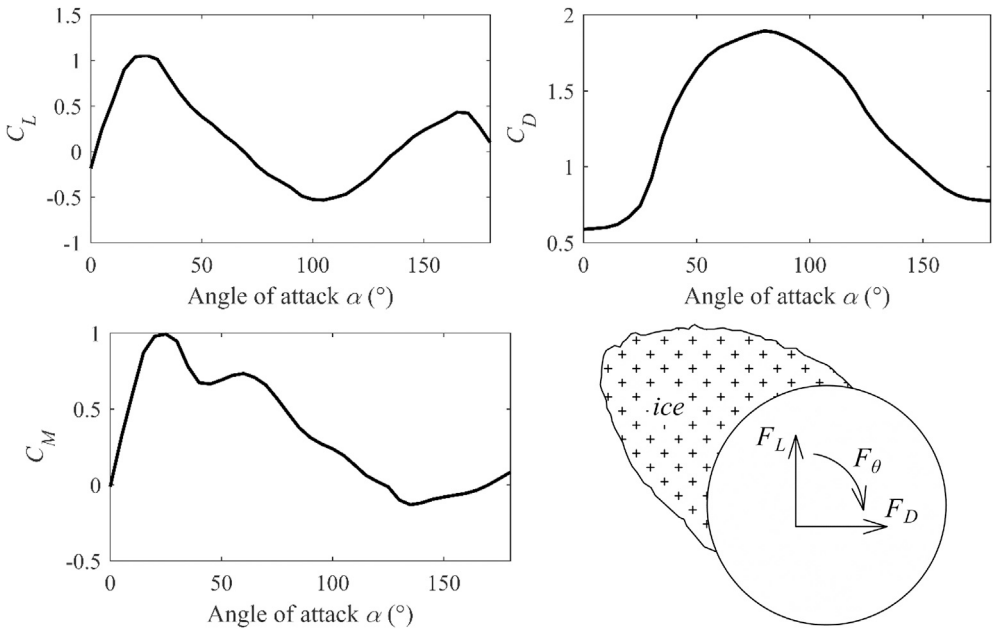


**Fig. 2.** Static force coefficients for a cable with heavy ice (Chabart and Lilien, 1998).

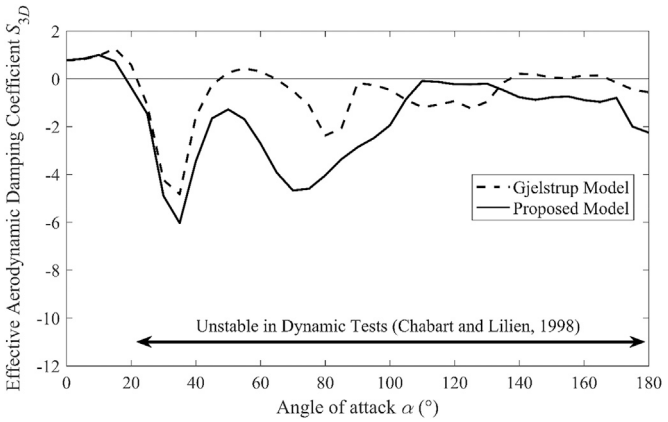


**Fig. 3.** Stability predicted by the present model and Gjelstrup model, and as observed in the dynamic tests. $U = 9$ m/s; $f_x = 0.960$ Hz, $f_y = 0.845$ Hz; $f_\theta = 0.865$ Hz; $\zeta_x = \zeta_y = 0.8\%$; $\zeta_\theta = 3.0\%$.

first and second columns.

In addition, there are aerodynamic stiffness terms, namely $-\frac{\partial \mathbf{F}}{\partial \theta}\Big|_{\theta_d=0}$, which could have an effect, especially for cross-sections with large side ratios or width to depth ratios. However, for the present work, the cross-sections investigated are normally referred to as compact cross-sections, i.e., the side ratios are normally less than 2, for which the effects of aerodynamic stiffness are usually assumed to be negligible compared to the structural stiffness (Gjelstrup and Georgakis, 2011). Therefore, the aerodynamic stiffness is excluded in the present analysis.

## 3. The effects of inertial coupling

In this section, the 3DOF model is first examined for its applicability in comparison with wind tunnel tests results (Chabart and Lilien, 1998) and a similar 3DOF model by Gjelstrup and Georgakis (2011), referred to as the Gjelstrup model hereinafter. Afterwards, the effects of the inertial coupling are investigated using the proposed 3DOF model.

### 3.1. Application of the proposed model

Due to a lack of experimental data of 3DOF dynamic tests of compact sections, the present analysis is largely based on data and results from the wind tunnel tests conducted by Chabart and Lilien (1998). The test section was an aluminium alloy conductor covered by thick silicone ice, giving large eccentricity. The force coefficients and the ice shape with the aerodynamic force sign conventions are depicted in Fig. 2:

Apart from the inertial coupling and aerodynamic damping, the 3DOF model developed by Gjelstrup and Georgakis (2011) also took into account both wind skew angle and Reynolds number effects. The stability is determined by the Routh-Hurwitz criterion, which, as discussed earlier, is convenient in finding out whether the system is stable or not but rather cumbersome for quantifying how unstable the system is. In addition, this model only succeeded in predicting part of the unstable region observed in the tests, i.e. from 25° to 45°, 70°–135° and 170°–180°, while galloping was found to occur from 20° to 180° in the dynamic experiments.

Through eigenvalue analysis, the stability of the proposed model, described by Eqs. (9), (10) and (12), is identified. Fig. 3 shows the galloping stability of the system, over the full range of angles of attack tested in the wind tunnel, as predicted by the present model and the Gjelstrup model. The observed unstable region in the experiments is also indicated. The stability is assessed in terms of the non-dimensional aerodynamic damping coefficient, $S_{3D}$, which is also employed in the galloping analyses by Nikitas and Macdonald (2014) and He and Macdonald (2016). It is defined as

$$S_{3D} = \frac{4m\omega_n\zeta_a}{\rho DU} \tag{13}$$

where $\zeta_a$ indicates the effective aerodynamic damping ratio, which is comparable to the structural damping ratios ($\zeta_x$, $\zeta_y$ and $\zeta_\theta$). A negative sign of $S_{3D}$ or $\zeta_a$ means galloping would occur if insufficient structural damping is provided. It should be noted the curves in Fig. 3 represent the most critical solution of the eigenvalue results, i.e. the minimum $S_{3D}$ of all three modes.

From Fig. 3, it is manifest that the proposed model predicts the whole unstable region observed in the experiments, which was reported by Chabart and Lilien (1998). It should be noted that all the parameters in the present analysis are consistent with those in (Gjelstrup and

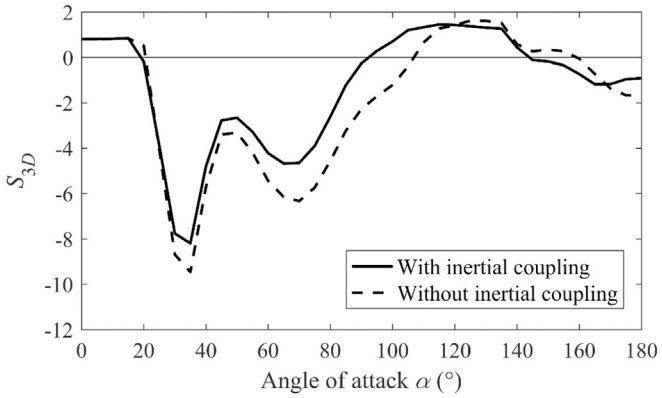


**Fig. 4.** Comparison of the galloping stability of the aeroelastically coupled cross-section with and without inertial coupling. Well-detuned system. $f_x = 0.96$ Hz, $f_y = 0.85$ Hz; $f_\theta = 1.54$ Hz; $\zeta_x = \zeta_y = 0.8\%$; $\zeta_\theta = 3.0\%$; $U = 9$ m/s.

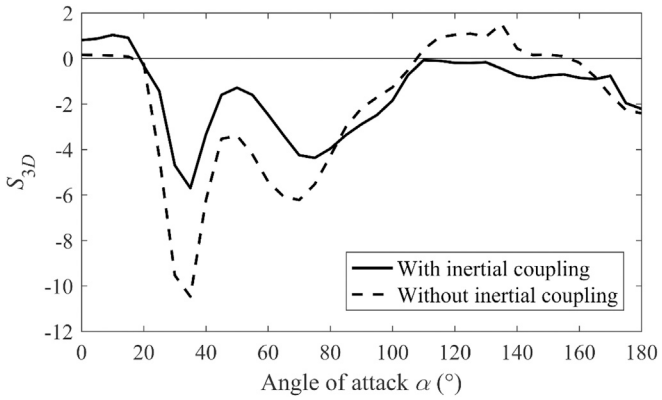


**Fig. 5.** Comparison of the galloping stability of the aeroelastically coupled cross-section with and without inertial coupling. Vertical and torsional frequencies closely tuned. $f_x = 0.995$ Hz, $f_y = 0.845$ Hz; $f_\theta = 0.865$ Hz; $\zeta_x = \zeta_y = 0.8\%$; $\zeta_\theta = 3.0\%$; $U = 9$ m/s.

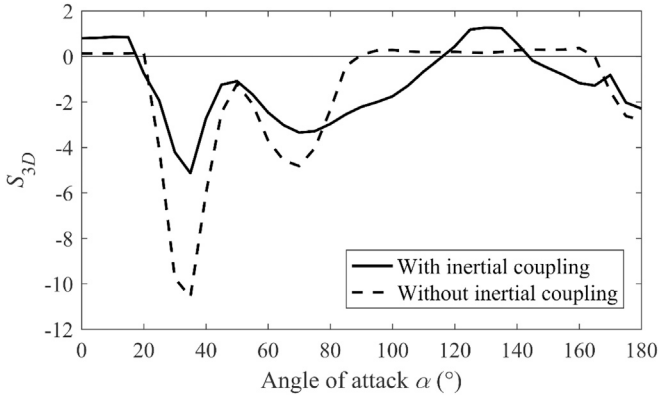


**Fig. 6.** Comparison of the galloping stability of the aeroelastically coupled cross-section with and without inertial coupling. All three frequencies perfectly tuned $f_x = f_y = f_\theta = 0.845$ Hz; $\zeta_x = \zeta_y = 0.8\%$; $\zeta_\theta = 3.0\%$; $U = 9$ m/s.

Georgakis, 2011) to be more comparable, except the definition of the aerodynamic centre. Moreover, their definitions of some of their angles are unclear, hence the reproduction of their results has to be under certain assumptions. Nevertheless, it seems that the main reason for the different predictions by the two similar models is the definition of the aerodynamic centre. Gjelstrup and Georgakis (2011) used the leading edge of the shape as the aerodynamic centre. However, after comparing several ways of defining the aerodynamic centre according to previous literature, it is found in the present analysis that the aerodynamic centre is chosen to be a fixed point on the principal axis in the $x$ direction with $L_a$ equal to the largest offset of the perimeter of the section from the elastic centre (i.e. the sum of the radius of the cable and the greatest ice thickness). Hence, the aerodynamic centre is basically the leading edge of the shape at 0° angle of attack and remains unchanged throughout the analysis. It is clear that with this assumption the results are greatly improved. In light of the fact that there is no theoretical position where the aerodynamic centre should be, it is suggested that for this particular cross-section, the chosen point appears to be the best choice.

### 3.2. Galloping stability of systems with and without inertial coupling

In order to further explore the significance of the inertial coupling, a series of numerical analyses are carried out, which can be divided into two approaches. The first approach is to compare two systems: (i) only aeroelastically coupled by the aerodynamic damping and (ii) coupled structurally by the inertial coupling as well as aeroelastically by the aerodynamic damping. The second approach, covered in the next section involves varying the offset of the centre of mass. The same cross-section tested by Chabart and Lilien (1998) is employed as an example. In their tests, two different plunge-to-torsion frequency ratios ($f_y/f_\theta$) were achieved through changing the position of the vertical springs.

Fig. 4 shows the numerical results of the setup with $f_y/f_\theta = 0.55$, in terms of the minimum non-dimensional aerodynamic damping coefficient, with and without the inclusion of inertial coupling.

The case illustrated in Fig. 4 represents a well-detuned system. The first impression is that the incorporation of the inertial coupling has only limited influence on the stability of the system. The two curves follow similar trends and the magnitudes are also close.

Fig. 5 shows the results for the same cross-section but with the vertical and torsional frequencies very close to each other ($f_y/f_\theta = 0.98$). As can be seen, the stability curves of the two systems also follow a similar trend with varying angles of attack. However, the difference in magnitude is often quite large in this case, especially around the most critical angles of attack, 35°. Including the mass eccentricity can lead to the stability curve shifting towards the stable or unstable side, depending on the position of the mass centre. For this particular shape, it implies the system would be more stable when the ice is at the upstream side. But when the ice accretion is on the leeward side, the inertial coupling seems to destabilise the system.

For the case with all the structural natural frequencies of the system perfectly tuned, with all the other parameters identical, the stability is shown in Fig. 6. Again, the stability curves, representing the two systems, show large discrepancies caused by the inertial coupling. For example, at the most unstable angle (around 35°), the system coupled by both inertial coupling and aerodynamic damping becomes much less unstable. In addition, from 90° to 160°, if the inertial coupling is not included, the system should be stable. However, once inertial coupling is incorporated, the system is only stable in the range of ~125°–135°. It is also clear that there are similarities between Figs. 5 and 6, especially for $\alpha < 90°$. The closely tuned and perfectly tuned cases are of particular interest for bundled conductors since they often have very close natural frequencies to each other.

In summary, the inertial coupling clearly has a great effect on the galloping stability, especially when the natural frequencies of the system are close.

### 3.3. The effects of varying inertial coupling

In this section, the effects of inertial coupling are investigated by varying the mass ratio between the ice and the cable, leading to a varying offset distance of the total mass centre from the elastic centre. The fundamental idea is to keep the shape, as well as the total mass of the

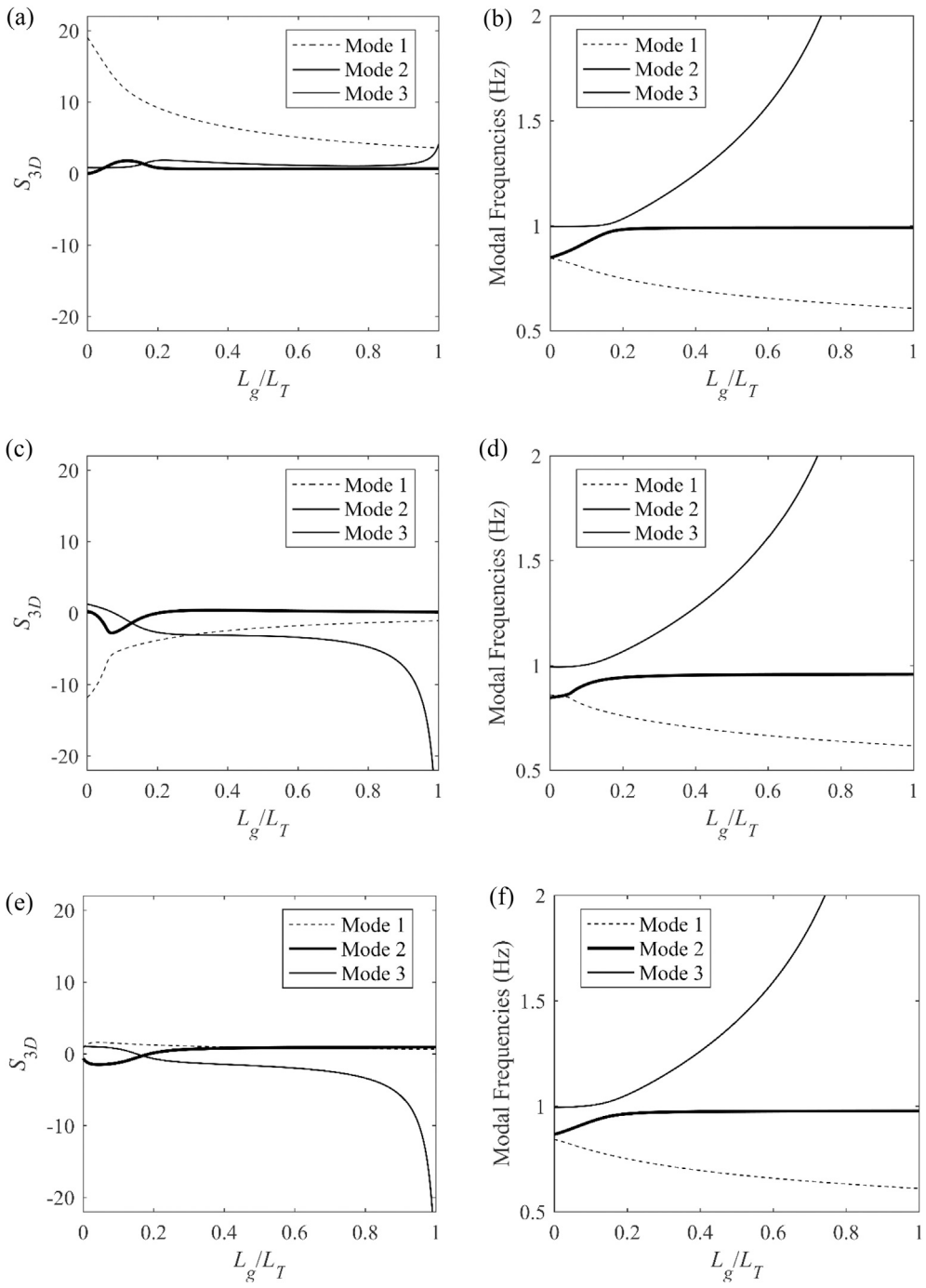


**Fig. 7.** Effects of varying the position of the centre of mass based on the cross-section from (Chabart and Lilien, 1998) at different angles of attack: (a, b). $\alpha = 10°$; (c, d). $\alpha = 30°$; (e, f). $\alpha = 160°$. $U = 9$ m/s; $f_x = 0.995$ Hz, $f_y = 0.845$ Hz; $f_\theta = 0.865$ Hz $\zeta_x = \zeta_y = \zeta_\theta = 0$.

cross-section unchanged, by only artificially changing the mass ratio of the ice to the whole cross-section to vary the location of the centre of mass (G) of the overall body. As has been defined earlier, the distance between the centre of mass the whole body (G) and the shear centre (O), which is also the centre of mass of the circular cylinder, is $L_g$. Herein, the distance between the centre of mass of the ice and that of the cable (O) is denoted herein by $L_T$. Hence, the mass ratio between the ice and the whole cross-section can be represented by $L_g/L_T$.

Fig. 7 illustrates the effects of increasing the inertial coupling at three different angles of attack. The figures on the left side show the effect on the stability of the each mode of the system, in terms of the non-dimensional aerodynamic damping coefficient, against the shift of the mass centre. The plots on the right side indicate the changes of the corresponding modal frequencies.

In general, Fig. 7 implies that the inertia effects due to the varying offset distance of the overall centre of mass can be linked to the effects of frequency tuning. For example, in Fig. 7(a), the stability curves, representing modes 1 and 2 accordingly, are far apart when the mass centre is not offset but quickly start to come together as $L_g/L_T$ increases until about 0.1. This indicates a detuning effect which can be verified by the corresponding modal frequency plot of Fig. 7(b). It is clear that the modal frequencies of modes 1 and 2 are initially very close to each other. Including the inertial coupling causes the modal frequencies of the modes 1 and 2 to diverge, while the stability of the modes rapidly converges.

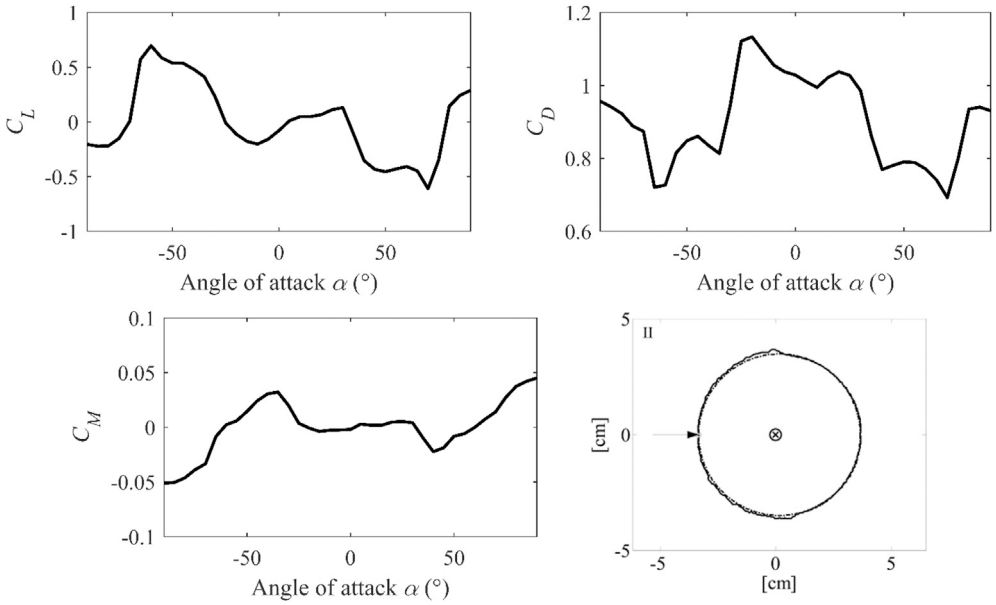


**Fig. 8.** Aerodynamic coefficients for Lightly iced cable with small eccentricity (Gjelstrup et al., 2012) (ice shape figure reproduced with kind permission of Techno-Press).

This is consistent with the classic pattern of tuning a 2DOF system, as has been shown by Nikitas and Macdonald (2014), i.e., at the perfect tuning point the stability curves of the two modes will be in either an attracting or repelling pattern and any detuning leads to the solutions changing asymptotically to the single-degree-of-freedom (SDOF) solutions. As the offset distance continues to increase, the frequency of mode 2 ceases growing around $L_g/L_T \approx 0.15$ and begins to approach 1 Hz asymptotically, while the frequency of mode 3, close to 1 Hz from $L_g/L_T = 0$, starts to increase. It seems that these two curves exhibit a typical "frequency veering" phenomenon. He and Macdonald (2015) investigated the effects of frequency tuning of the 3DOF system, coupled by aerodynamic damping, and suggested that frequency veering occurs whenever the so-called "complex motion" occurs. The term "complex motion" has been used by many researchers (Jones, 1992; Carassale et al., 2005; Macdonald and Larose, 2008a; Nikitas and Macdonald, 2014; He and Macdonald, 2016) to signify a special solution of a coupled system with resonant structural natural frequencies, where two modes with different modal frequencies have identical stability. Using a perturbation approach, Luongo and Piccardo (2005) identified the similarity between this so-called "complex response" and double Hopf bifurcation. As can be seen from the stability curves (Fig. 7(a)), the stability curves corresponding to the two veering modes, indeed intersect at the frequency veering point. It is noted that modes 2 and 3 cross at $L_g/L_T \approx 0.05$ but without veering, which is believed to be due to the frequencies of modes 1 and 2 are almost identical while the modal frequency of mode 3 can be regarded as detuned. Hence, the interaction between modes 1 and 2 is more essential.

Similar features of both stability and frequency curves can also be found in Fig. 7(c) and (d). Fig. 7(c) indicates modes 1 and 2 have a similar tuning pattern to those in Fig. 7(a), i.e. a repelling pattern when the system is perfectly tuned. Once the eccentricity is introduced, the modal frequencies of these two modes are detuned, causing the stability curves to move quickly towards each other. As the mass centre continues to shift away, frequency veering occurs between modes 2 and 3 leading to the crossing of the corresponding stability curves. It is very interesting to notice the rapid changes of the stability of certain modes even when the eccentricity introduced is very small. For instance, mode 2, which is near the stability boundary but stable, quickly becomes very unstable when the eccentricity is only about 5%.

Fig. 7(e) and (f) again illustrate both the tuning effects and the frequency veering phenomenon, as explained above. This time, the close tuning of modes 1 and 2 leads to an attracting pattern of the stability curves. When the inertial coupling is increased, modal frequencies of modes 1 and 2 are detuned, leading to the divergence of the corresponding stability curves. As a result, the stability curve of mode 2 goes down to lower values away from the stability boundary as the eccentricity increases. When the inertial coupling is strong enough, frequency veering occurs, resulting in the stability curves of mode 2 reversing back towards the stability boundary. It intersects with the curve representing the stability of mode 3, which is also an expected feature for frequency veering.

Another important feature of all of the stability curves is that even very small eccentricity can cause a significant change of the system stability. In all of the plots, the stability of at least one of the modes changes rapidly as the position of the centre of mass starts to move away from the shear centre. It is important to note that the stability of the system can experience considerable changes due to the inertial coupling only, for no change in the aerodynamics, even for a small offset of the centre of mass. For instance, if a small protuberance is attached to a circular cylinder, it is well known that the modification of the aerodynamics could lead to instability. However, the associated small offset of the centre of mass could also be important in changing the stability. This possibility is now explored further with a lightly iced cable, the centre of mass of which is manually offset by a very small distance.

Gjelstrup et al. (2012) conducted a series of wind tunnel tests on circular cylinders covered by four different ice coatings. The test setup allowed for plunge and torsion but the horizontal motion was fully restrained. The test results were used to compare with their analytical model (Gjelstrup and Georgakis, 2011), using the Routh-Hurwitz criterion. The lightly iced cable employed in the present analysis is the shape II, plotted in Fig. 8, which has a mean ice thickness of only 1.4% of the diameter of the cable. Consequently, the effects of mass eccentricity were considered to be negligible in their numerical examinations reported in Gjelstrup et al. (2012). The aerodynamic coefficients are also provided in Fig. 8.

Firstly, an eigenvalue analysis is conducted using the proposed model but only including the across-wind ($y$) and torsional ($\theta$) degrees of freedom, based on this shape with all the parameters consistent with the analysis by Gjelstrup et al. (2012). Then, the same analysis is repeated but a small offset of the centre of mass will be numerically created to introduce inertial coupling. The offset distance is 5% of the cable diameter from the elastic centre (shear centre). As a result, the mass matrix

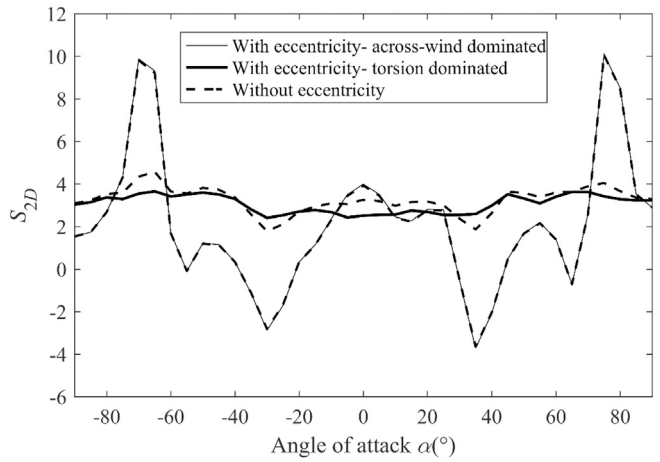


**Fig. 9.** Comparison of galloping stability of a lightly iced cable with and without mass eccentricity. $U = 41$ m/s; $f_y = 1.63$ Hz; $f_\theta = 4.99$ Hz; $\zeta_y = 0.8\%$; $\zeta_\theta = 4.3\%$.

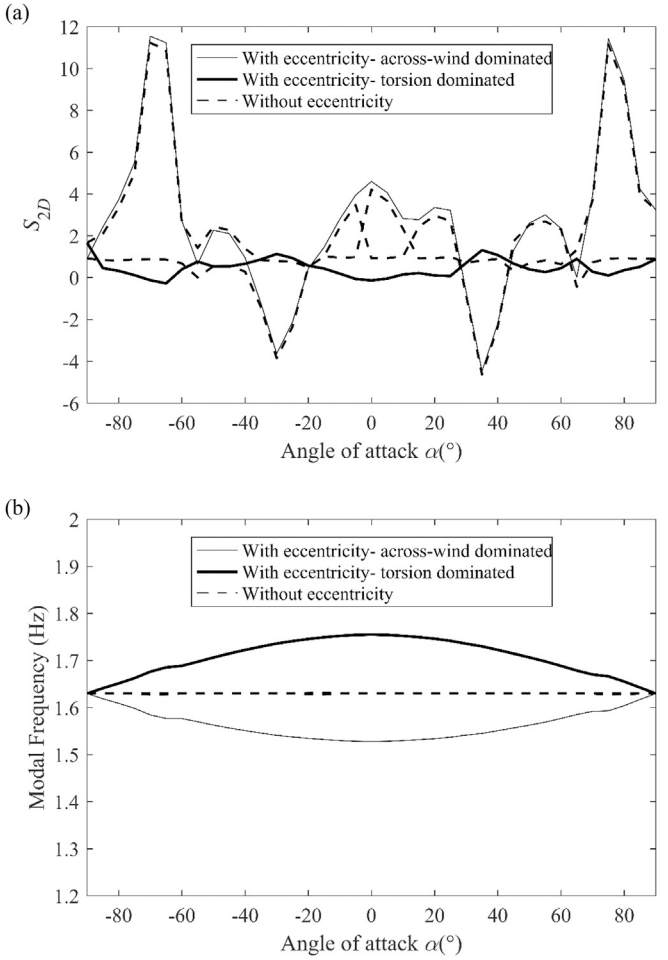


**Fig. 10.** Comparison of galloping stability of a lightly iced cable with and without mass eccentricity: (a) the stability expressed in terms of the non-dimensional aerodynamic damping; (b) modal frequencies. $U = 41$ m/s; $f_y = f_\theta = 1.63$ Hz; $\zeta_y = 0.8\%$; $\zeta_\theta = 4.3\%$.

becomes non-diagonal. Also, the mass polar moment of inertia is slightly different. The results of both cases are compared and illustrated in Fig. 9. It should be mentioned that $S_{2D}$, equivalent to $S_{3D}$ in the preceding section, is used herein since the model is a 2DOF one.

As can be seen from Fig. 9 for a system with well separated natural frequencies, the incorporation of such small eccentricity seems to have negligible influence on the across-wind dominated mode while there is a significant effect on the torsion dominated mode. Despite the difference for the torsion dominated mode, it remains stable for all angles of attack, while in any case, the across-wind dominated mode is unstable for certain angles of attack. Considering the modal frequencies, the changes were minor. There was a negligible shift in the frequency of the across-wind dominated mode and the frequency of the torsion dominated mode changed only up to 1.05% due to the inertial coupling.

Following the preceding analysis, another case is also investigated where the same system has resonant structural natural frequencies, illustrated in Fig. 10. The figure shows that for the perfectly tuned system, the stability curves of both modes show a noticeable difference between the two cases, i.e., with and without small eccentricity. With regard to the overall stability of the system, the behaviour at the most unstable angles of attack, namely about ±35°, is almost the same for both cases. However, including eccentricity may lead to different unstable regions when the system is not far from the stability boundary, i.e., when $S_{2D}$ is close to 0. For example, when only aerodynamic damping is included, the system is slightly unstable at about 65°. After introducing small eccentricity, at 65°, the system is just on the stability boundary, which means it should be neutrally stable. On the other hand, at approximately −65°, the aerodynamically coupled case indicates the system is clearly stable but once the mass offset is introduced, the system becomes unstable at that angle in the torsion dominated mode.

In summary, the inertial coupling can exert significant influence on the stability of a system for both perfectly tuned and detuned cases. Even if the offset of the centre of mass is small, the effects on the stability can still be substantial.

## 4. Analytical investigation of a perfectly tuned system with inertial coupling

The preceding sections have demonstrated the importance of the inertial coupling for both detuned and perfectly tuned systems based on numerical eigenvalue analysis. It could be more useful for practical purposes and more insightful to have analytical solutions. However, due to the complex nature of the problem, it is difficult to obtain simple analytical solutions for a system with arbitrary tuning. In the first part of this section, analytical expressions of the eigenfrequencies along with the associated eigenvectors are derived for a perfectly tuned 3DOF system structurally coupled by mass inertia without the presence of wind. As mentioned earlier, the perfectly tuned case is of use for bundled conductors which have very close natural frequencies for all 3 degrees of freedom. Thenceforth, an approximate solution is proposed in the second part for the onset of galloping for a perfectly tuned 3DOF system coupled by aerodynamic damping and inertial coupling. The structural damping ratio in the whole section is neglected for simplicity since the structural damping only makes the system more stable.

### 4.1. Without the presence of wind

With the structural matrices defined as for Eq. (9), the eigenvalues of a system with only inertial coupling, with no wind or structural damping can be obtained by

$$\left| -\omega^2\mathbf{M} + \mathbf{K} \right| = 0 \tag{14}$$

where $\omega$ is the eigenfrequency of the inertially coupled system. It should be noted the structural natural frequencies without coupling, namely $\omega_x$, $\omega_y$ and $\omega_\theta$, are all set to be $\omega_n$ for a perfectly tuned system. Hence, Eq. (14) can be expanded into:

$$\left(\omega^2 - \omega_n^2\right)\left(\left(L_g - r\right)\omega^2 + r\omega_n^2\right)\left(\left(L_g + r\right)\omega^2 - r\omega_n^2\right) = 0 \tag{15}$$

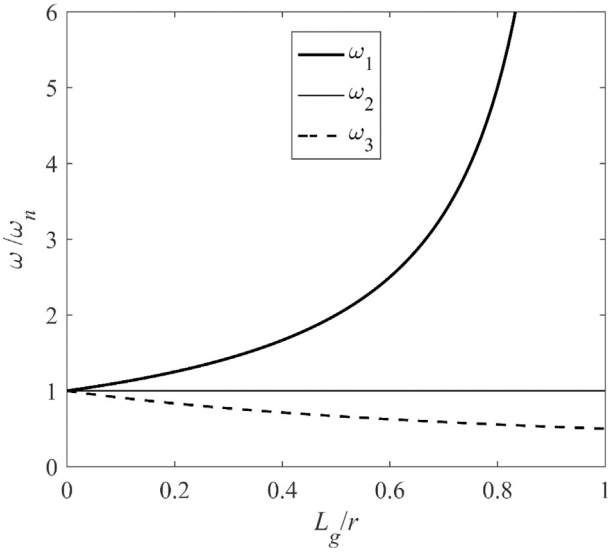


**Fig. 11.** The effects of the inertial coupling on the system eigenfrequencies of a perfectly tuned 3DOF system with no wind.

The three solutions for the eigenvalues ($\omega$), $\omega_1$, $\omega_2$, $\omega_3$ along with their associated eigenvectors, $\boldsymbol{\phi}_1$, $\boldsymbol{\phi}_2$, $\boldsymbol{\phi}_3$, are:

$$\omega_1^2 = \frac{r}{r-L_g}\omega_n^2,\ \boldsymbol{\phi}_1 = \begin{Bmatrix} -r\sin(\alpha_g+\theta_0) \\ -r\cos(\alpha_g+\theta_0) \\ 1 \end{Bmatrix},$$

$$\omega_2^2 = \omega_n^2,\ \boldsymbol{\phi}_2 = \begin{Bmatrix} -\cot(\alpha_g+\theta_0) \\ 1 \\ 0 \end{Bmatrix},$$

$$\omega_3^2 = \frac{r}{r+L_g}\omega_n^2,\ \boldsymbol{\phi}_3 = \begin{Bmatrix} r\sin(\alpha_g+\theta_0) \\ r\cos(\alpha_g+\theta_0) \\ 1 \end{Bmatrix}.$$

An illustration of the normalised eigenfrequencies with varying $L_g/r$ is shown in Fig. 11, which demonstrates the significance of the inertial coupling.

As can be seen, $\omega_3$ decreases as the inertial coupling increases while $\omega_1$ has an opposite trend. Based on the eigenvectors, the trajectories of the motion in each mode are plotted in Fig. 12, for an offset angle of the centre of mass of 30° as an example. Mode 1 (Fig. 12(a)) represents a rotation about a point that is between the centre of mass (G) and the elastic centre (O), which moves closer to G with increasing mass offset. Therefore, polar moment of inertia about the point decreases, so the modal frequency should increase with increasing offset. On the other hand, the eigenvector of Mode 3 (Fig. 12(c)) indicates motion about a point the same distance from O but in the opposite direction. Hence, the polar moment of inertia about the point increases and the natural frequency decreases as the inertial coupling increases. Mode 2 (Fig. 12(b)) involves purely translational motion along the line ($\overline{OG}$) connecting the two centres, which is not affected by the inertial coupling, giving a modal frequency equal to the uncoupled natural frequencies of the system. It is also evident that the amplitude ratio of the translational motions of Modes 1 and 3 always follow the same relation, i.e. the horizontal amplitude over the vertical one always equals $\tan(\alpha_g+\theta_0)$.

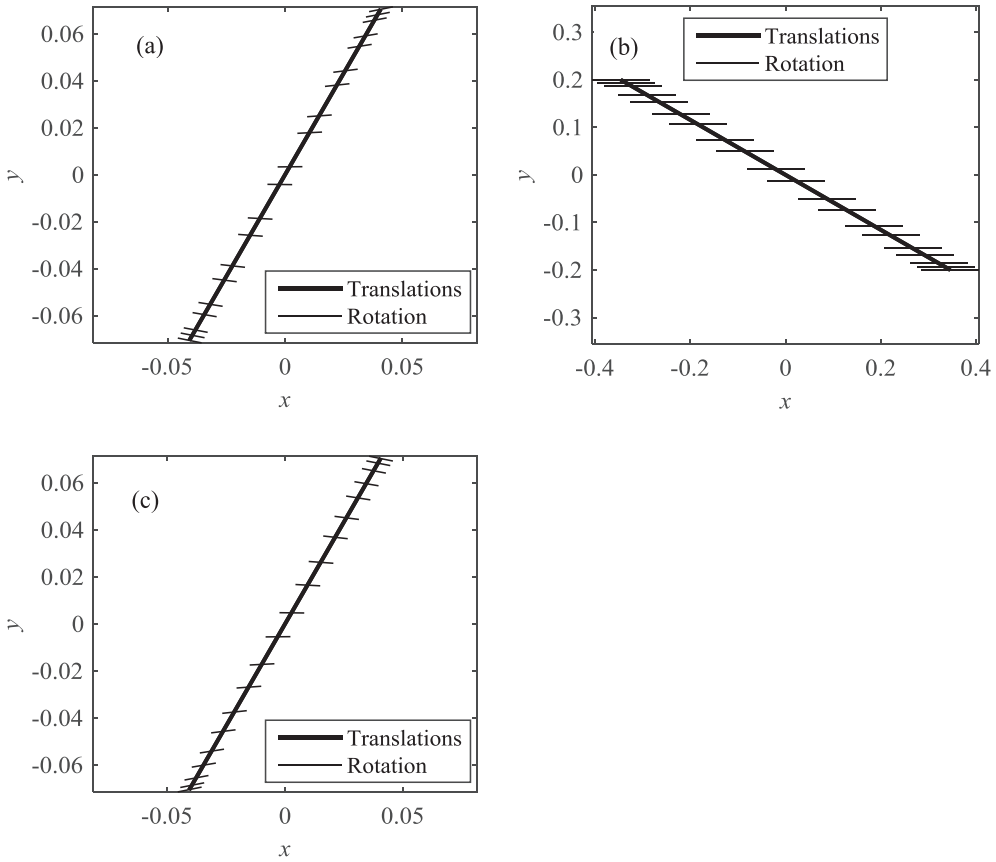


**Fig. 12.** Trajectories of motion in the 3 modes: (a) Mode 1; (b) Mode 2; (c) Mode 3. The 'rotation' lines show snapshots of the orientation of the body at equal time intervals over the vibration cycle.

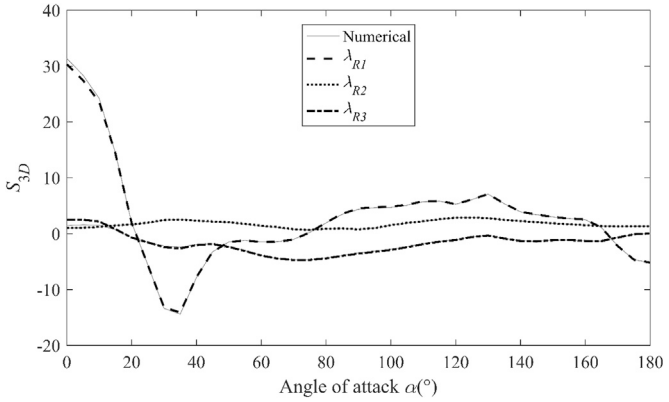


**Fig. 13.** Comparison between the proposed closed-form solutions and the numerical results for a heavily iced cable (Chabart and Lilien, 1998). $f_x = f_y = f_\theta = f_n = 1$ Hz, $\zeta_x = \zeta_y = \zeta_\theta = 0$, $U = 9$ m/s. Offset distance of the centre of mass is 7.7% of the cable diameter.

### 4.2. Approximate solutions for galloping of a 3DOF body coupled by both inertial coupling and aerodynamic damping

With the above insights of the effects of inertial coupling with no wind, the more general case, incorporating both inertial coupling and aerodynamic damping, is examined. Using the same 3DOF model, as well as the mass and stiffness matrices, the space state matrix **A**, after adding the aerodynamic damping matrix, is:

$$\mathbf{A} = \begin{bmatrix} \mathbf{0} & \mathbf{I} \\ -\mathbf{M}^{-1}\cdot\mathbf{K} & -\mathbf{M}^{-1}\cdot\mathbf{C_a} \end{bmatrix} \tag{16}$$

The structural damping is neglected in the present analysis to make the problem tractable, noting that the structural damping is normally small in practice (Chen and Kareem, 2006) and that adding structural damping will always increase the stability.

Following He and Macdonald (2016), the aerodynamic damping matrix can be expressed as:

$$\mathbf{C_a} = \frac{\rho D U}{2}\begin{bmatrix} 1 & 0 & 0 \\ 0 & 1 & 0 \\ 0 & 0 & r \end{bmatrix}\mathbf{S_a}\begin{bmatrix} 1 & 0 & 0 \\ 0 & 1 & 0 \\ 0 & 0 & r \end{bmatrix} \tag{17}$$

where $\mathbf{S_a}$ is a non-dimensional matrix, given by (He and Macdonald, 2016):

$$\begin{aligned} \mathbf{S_a} &= \begin{bmatrix} S_{xx} & S_{xy} & S_{x\theta} \\ S_{yx} & S_{yy} & S_{y\theta} \\ S_{\theta x} & S_{\theta y} & S_{\theta\theta} \end{bmatrix} \\ &= \begin{bmatrix} 2C_D & 2C_L & (C_L' + C_D) & (C_L - C_D') & 0 & 0 \\ 2C_L & -2C_D & (C_L - C_D') & -(C_L' + C_D) & 0 & 0 \\ 0 & 0 & 0 & 0 & 2\kappa C_M & \kappa C_M' \end{bmatrix} \\ &\times \begin{bmatrix} c^2 & cs & \varepsilon s_{\alpha\theta\gamma}\, c \\ -cs & -s^2 & -\varepsilon s_{\alpha\theta\gamma}\, s \\ s^2 & -cs & -\varepsilon c_{\alpha\theta\gamma}\, s \\ cs & -c^2 & -\varepsilon c_{\alpha\theta\gamma}\, c \\ c & s & \varepsilon s_{\alpha\theta\gamma} \\ -s & c & \varepsilon c_{\alpha\theta\gamma} \end{bmatrix} \end{aligned} \tag{18}$$

where $\kappa = D/r$ and $\varepsilon = L_a/r$.

The characteristic polynomial of the system is given by:

$$|\mathbf{A} - \lambda\mathbf{I}| = 0 \tag{19}$$

where $\lambda$ are the complex eigenvalues of the problem.

Eq. (19) is a lengthy 6th order equation, which theoretically could be decomposed into the form of the product of three quadratic equations, each representing one of the three modes with complex conjugate roots. Therefore, an approximate equation in such a form is proposed:

$$\left(\lambda^2 + b_1\cdot\lambda + \frac{r}{r - L_g}\omega_n^2\right)\left(\lambda^2 + b_2\cdot\lambda + \omega_n^2\right)\left(\lambda^2 + b_3\cdot\lambda + \frac{r}{r + L_g}\omega_n^2\right) \approx 0 \tag{20}$$

The eigenfrequencies, i.e. the third term in each pair of brackets in Eq. (20), assuming low damping, are estimated to be equal to those for the no wind condition, calculated from Eq. (15). This assumption is in agreement with Chen and Kareem (2006). They found that for low levels of damping, which is generally the case in flutter or galloping analysis, the aerodynamically uncoupled natural frequencies can be used to estimate the coupled modal frequencies in presence of wind.

After expanding Eq. (20), the coefficients of each order of $\lambda$ are represented by mathematical combinations of three unknowns, $b_1$, $b_2$ and $b_3$. By comparing these coefficients with those in the characteristic polynomial derived from Eq. (19), a set of equations can be established to solve for those unknowns. From observation of the expanded Eq. (20), the coefficients of $\lambda^5$ and $\lambda$ are linear relations of the three unknowns. Furthermore, the coefficient of $\lambda^3$ also contains linear relations of the three unknowns, with only one higher order term, i.e. $b_1b_2b_3$. This term is equivalent to the product of the real part of all the eigenvalues. Since the real part of the eigenvalues gives the overall damping of each degree of freedom of the system, which is generally fairly small, the product of them is hence quite close to zero. The corresponding coefficient in Eq. (19) contains an equivalent "higher order" term, namely the determinant of the damping matrix ($|\mathbf{C_a}|$) which is always 0. Thus, $b_1b_2b_3$ and $|\mathbf{C_a}|$ can be cancelled out from both sides of the equation. Consequently, a third linear relation between the three unknowns can be obtained. By solving the three linear equations in $b_1$, $b_2$ and $b_3$, the real part of the eigenvalues ($\lambda_R$) of each mode can be derived, since only the instability threshold is of interest, as

$$\lambda_{R1} = -\frac{b_1}{2} \approx \frac{\rho D U}{8m}\frac{r}{(r - L_g)}(d_1 + d_2) \tag{21}$$

$$\lambda_{R2} = -\frac{b_2}{2} \approx -\frac{\rho D U}{4m}\left(S_{xx} + S_{yy} + S_{\theta\theta} + d_1\right) \tag{22}$$

$$\lambda_{R3} = -\frac{b_3}{2} \approx \frac{\rho D U}{8m}\frac{r}{(r + L_g)}(d_1 - d_2) \tag{23}$$

where

$$\begin{aligned} d_1 &= -\{S_{xx}\sin^2(\alpha_g + \theta) + S_{yy}\cos^2(\alpha_g + \theta) + (S_{xy} + S_{yx})\sin(\alpha_g + \theta) \\ &\cos(\alpha_g + \theta) + S_{\theta\theta}\} \\ d_2 &= (S_{\theta y} + S_{y\theta})\cos(\alpha_g + \theta) + (S_{x\theta} + S_{\theta x})\sin(\alpha_g + \theta) \end{aligned}$$

For stability, a positive real part indicates an unstable mode while a negative value means the mode is stable. Hence, the galloping stability can be assessed using the maximum of the three simple expressions (Eqs. (21)–(23)), or the minimum one, if the equivalent non-dimensional aerodynamic damping coefficients are used ($S_{3D} = -4m\lambda_R/\rho DU$).

### 4.3. Validation and application of the proposed analytical solutions

In this section, the proposed approximate solution is validated against the exact numerical results. The two examples, employed in the previous sections, namely the iced cables tested by Chabart and Lilien (1998) and Gjelstrup et al. (2012), are investigated.

Firstly, the cable with large ice coating examined by Chabart and Lilien (1998) is utilised. Since the proposed approximate solutions only apply for perfectly tuned structural natural frequencies (before the inertial coupling is introduced), they are all set to be $f_n = 1$ Hz. This is quite

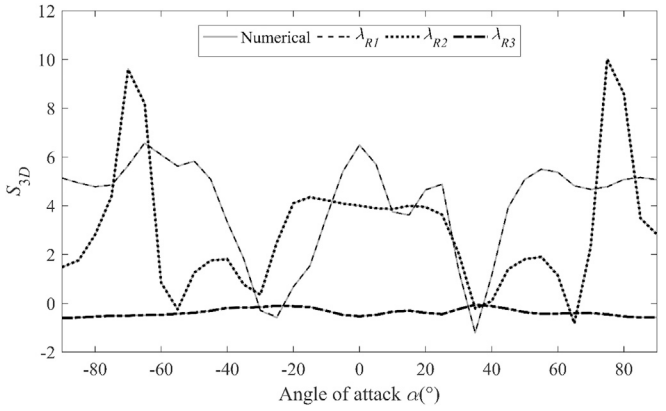


**Fig. 14.** Comparison between the proposed closed-form solutions and the numerical results on a lightly iced cable (Gjelstrup et al., 2012). $f_x = f_y = f_\theta = f_n = 1.63$ Hz, $\zeta_x = \zeta_y = \zeta_\theta = 0$, $U = 41$ m/s, $L_g/L_T = 0.1$.

close to the original frequencies of the dynamic test cable. All the other parameters are the same as those used in the previous analyses.

The comparison of the stability predictions given by the proposed approximate solutions and the exact numerical results is presented in Fig. 13, in terms of the non-dimensional aerodynamic damping coefficient, $S_{3D}$.

As can be seen in Fig. 13, the proposed approximate solutions are generally in excellent agreement with the results of the numerical eigenvalue analysis. Only for angles of attack from 0° to about 10° do noticeable discrepancies occur. The predictions throughout the whole unstable region are excellent.

To further confirm the validity of the approximate solution, the lightly iced cable (Gjelstrup et al., 2012) is also checked. In this case, all three degrees of freedom are included and the natural frequencies (before introducing inertial coupling) are all tuned to be $f_n = 1.63$ Hz. Moreover, the offset of the centre of mass is manually set to be 10% of the diameter with an offset angle of 0°. All the other parameters are as for the actual test data. The results comparison is shown in Fig. 14.

Fig. 14 clearly demonstrates the excellent agreement between the approximate solutions and the exact results. Further numerical exploration has shown that the agreement still remains very good for a wide range of offset lengths and offset angles of the centre of mass. Hence, for all the cases considered, the simple approximate solutions in Eqs. (21)-(23) provide very good predictions of the galloping stability of 3DOF perfectly tuned systems, including inertial effects considered.

## 5. Conclusions

The effects of incorporating inertial coupling on the galloping stability of a 3DOF system coupled also by aerodynamic damping are investigated in the present work. The inertial coupling terms are first derived along with the quasi-steady aerodynamic damping matrix based on a two-dimensional 3DOF model. The proposed 3DOF model is then used to assess the stability of a heavily iced transmission line conductor, the results of which are compared with the observations in dynamic tests, as well as the predictions from a previous analytical model. The proposed model provides better agreement with the test results than the previous model. The significance of the inertial coupling is investigated through two approaches, showing a strong influence on the galloping stability for both detuned and perfectly tuned systems, especially for the latter. Analytical expressions of the eigenvalues and eigenvectors of a perfectly tuned 3DOF system with inertial coupling, neglecting structural damping, are derived, based on which analytical approximations for the onset of galloping is proposed for the special case of perfect tuning. The predictions of the approximate solutions are validated through two example cross-sections with different ice shapes, demonstrating excellent agreement with the exact numerical calculations.

## Acknowledgement and data access statement

The first author was supported by a University of Bristol Postgraduate Research Scholarship. All data used in this study are available in the cited papers.

## References

Blevins, R.D., 1994. Flow-induced Vibration. Van Nostrand Reinhold, New York.
Blevins, R.D., Iwan, W.D., 1974. The galloping response of a two-degree-of-freedom system. J. Appl. Mech. 41, 1113.
Carassale, L., Freda, A., Piccardo, G., 2005. Aeroelastic forces on yawed circular cylinders: quasi-steady modeling and aerodynamic instability. Wind Struct. 8, 373–388.
Chabart, O., Lilien, J.L., 1998. Galloping of electrical lines in wind tunnel facilities. J. Wind Eng. Ind. Aerodyn. 74–76, 967–976.
Chen, X.Z., Kareem, A., 2006. Revisiting multimode coupled bridge flutter: some new insights. J. Eng. Mech. ASCE 132, 1115–1123.
Demartino, C., Ricciardelli, F., 2015. Aerodynamic stability of ice-accreted bridge cables. J. Fluids Struct. 52, 81–100.
Den Hartog, J., 1932. Transmission line vibration due to sleet. Trans. Am. Inst. Electr. Eng. 4, 1074–1076.
Gjelstrup, H., Georgakis, C.T., 2011. A quasi-steady 3 degree-of-freedom model for the determination of the onset of bluff body galloping instability. J. Fluids Struct. 27, 1021–1034.
Gjelstrup, H., Georgakis, C.T., Larsen, A., 2012. An evaluation of iced bridge hanger vibrations through wind tunnel testing and quasi-steady theory. Wind Struct. 15, 385–407.
He, M., Macdonald, J., 2015. Tuning effects of a 3dof aeroelastically coupled system: a study based on quasisteady theory. In: 14th International Conference on Wind Engineering. Porto Alegre, Brazil.
He, M., Macdonald, J.H.G., 2016. An analytical solution for the galloping stability of a 3 degree-of-freedom system based on quasi-steady theory. J. Fluids Struct. 60, 23–36.
Jones, K.F., 1992. Coupled vertical and horizontal galloping. J. Eng. Mech. ASCE 118, 92–107.
Luongo, A., Piccardo, G., 2005. Linear instability mechanisms for coupled translational galloping. J. Sound Vib. 288, 1027–1047.
Macdonald, J.H.G., Larose, G.L., 2006. A unified approach to aerodynamic damping and drag/lift instabilities, and its application to dry inclined cable galloping. J. Fluids Struct. 22, 229–252.
Macdonald, J.H.G., Larose, G.L., 2008a. Two-degree-of-freedom inclined cable galloping—part 1: general formulation and solution for perfectly tuned system. J. Wind Eng. Ind. Aerodyn. 96, 291–307.
Macdonald, J.H.G., Larose, G.L., 2008b. Two-degree-of-freedom inclined cable galloping—part 2: analysis and prevention for arbitrary frequency ratio. J. Wind Eng. Ind. Aerodyn. 96, 308–326.
Modi, V.J., Slater, J.E., 1983. Unsteady aerodynamics and vortex induced aeroelastic instability of a structural angle section. J. Wind Eng. Ind. Aerodyn. 11, 321–334.
Nakamura, Y., Mizota, T., 1975. Torsional flutter of rectangular prisms. J. Eng. Mech. Div. ASCE 101, 125–142.
Nikitas, N., Macdonald, J.H.G., 2014. Misconceptions and generalizations of the den hartog galloping criterion. J. Eng. Mech. ASCE 140, 04013005.
Païdoussis, M.P., Price, S.J., De Langre, E., 2010. Fluid-structure Interactions: Cross-flow-induced Instabilities. Cambridge University Press.
Piccardo, G., Pagnini, L.C., Tubino, F., 2014. Some research perspectives in galloping phenomena: critical conditions and post-critical behavior. Continuum Mech. Thermodyn. 27, 261–285.
Slater, J.E., 1969. Aeroelastic Instability of a Structural Angle Section. PhD Thesis. University of British Columbia.
Wang, J.W., Lilien, J.L., 1998. Overhead electrical transmission line galloping - a full multi-span 3-dof model, some applications and design recommendations. IEEE Trans. Power Deliv. 13, 909–916.
Yu, P., Desai, Y.M., Shah, A.H., Popplewell, N., 1993a. Three-degree-of-freedom model for galloping. Part I: Formulation. J. Eng. Mech. ASCE 119, 2404–2425.
Yu, P., Desai, Y.M., Popplewell, N., Shah, A.H., 1993b. Three-degree-of-freedom model for galloping. Part II: Solutions. J. Eng. Mech. ASCE 119, 2426–2448.
Yu, P., Popplewell, N., Shah, A.H., 1995a. Instability trends of inertially coupled galloping: Part i: Initiation. J. Sound Vib. 183, 663–678.
Yu, P., Popplewell, N., Shah, A.H., 1995b. Instability trends of inertially coupled galloping: Part ii: periodic vibrations. J. Sound Vib. 183, 679–691.